B21090

Anna Ioannou, Ioanna Vareli, Andreas Kaltzoglou and Ioannis Koutselas*

Synthesis, characterization and optoelectronic properties of 2D hybrid $RPbX_4$ semiconductors based on an isomer mixture of hexanediamine-based dications

Corresponding author: Ioannis Koutselas, Materials Science Department, School of Natural Sciences, University of Patras, Patras, 26504, Greece; e-mail: ikouts@upatras.gr

Anna Ioannou: Materials Science Department, School of Natural Sciences, University of Patras, Patras, 26504, Greece

Ioanna Vareli: Materials Science Department, School of Natural Sciences, University of Patras, Patras, 26504, Greece, and Department of Materials Science and Engineering, University of Ioannina, Ioannina, 45110, Greece

Andreas Kaltzoglou: Theoretical and Physical Chemistry Institute, National Hellenic Research Foundation, Athens, 11635, Greece

Abstract: Three new hybrid two-dimensional (2D) organic-inorganic semiconductors are presented, which contain lead halides and a mixture of hexanediamine-based isomers in the stoichiometry [2,2,4*(2,4,4)*-trimethyl-1,6-hexanediamine]PbX_4 (X = I, Br, Cl). These hexanediamine derivatives, with attached methyl groups at the carbon backbone of both isomers, determine the packing of the organic layers between the inorganic 2D sheets, while the optical absorption and photoluminescence spectra reveal excitonic peaks at *T* =

77 K and room temperature. The as-synthesized semiconductors were stored for three years in the dark and under low humidity and were examined again and the results were compared to those of the fresh materials. The chloride analogue, after the 3-year storage, displays white-like luminescence. The use of isomer and racemic mixtures in the organic component to form hybrid organic-inorganic semiconductors is an efficient method to alter the properties of 2D perovskites by tuning the isomers' chemical functionalities. Finally, the absence of strong and sharp excitonic absorption and photoluminescence signals for the current 2D hybrids compared to analogous 2D compounds is discussed.

Keywords: low dimensional hybrid organic-inorganic perovskites; exciton; chirality; luminescence

Introduction

Materials exhibiting the perovskite structure have been known since the 19th century [1]. However, the low-dimensional organic-inorganic semiconductors (LD HOIS) based on metal halide perovskites have redrawn the attention of the research community over the past ten years, thanks to their tunable optoelectronic properties, their low cost, simple synthesis as well as the plethora of their new applications [2–8]. Since 2009, when the first perovskite photovoltaic device was reported [9], the photovoltaic power conversion efficiency has reached 25. 2%, which is close to the silicon-based single-junction photovoltaics [10], while perovskite/silicon tandem solar cells have shown efficiencies up to 29. 1% [10–14]. HOIS research has focused their wide applicability for optoelectronic applications in the semiconductor industry, for

application in luminescence, photodetection, chemical sensors, and photocatalysis, among others [15–24].

The general chemical formula of halide perovskites is $R_yM_xX_z$, where R is typically a large or small mono/di-valent cation, M is a divalent cation, usually Pb or Sn, while X is Cl, Br or I [25]. This leads to hundreds of chemical compounds, but the main trend [26–37] is to incorporate either methylammonium or formamidinium ions as the cation, Pb as the metal and iodine or a mixture of halides as the anion, at least for solar cells. Their structure usually consists of face- or corner-sharing MX_6 octahedra where the organic cations fill the voids among the octahedra in the 3D systems; in the 2D perovskites the organic molecules stabilize the 2D octahedra-based layers [38]. By adjusting the chemical composition of a variety of perovskites, their optical/electronic properties can be tuned [39,40]. Moreover, their structures can be tuned to behave as 3D, 2D, 1D, 0D or intermediate dimensionalities semiconductors [6–43].

A simple method to produce LD HOIS is to introduce large organic molecules as cations [44–53]. In this case the contributing function of the R-site cation, besides leading the 2D (lamellar) formation, is providing anisotropy to a variety of properties as well as to carrier properties and diffusion lengths for which details have been reported numerous times [54–57]. Also, a recent example is the use of $[NH_3(CH_2)_6NH_3]PbI_4$ in perovskites in solar cells, since its 2D structure passivates the humidity sensitive 3D mixed-anion and mixed-cation perovskite, that acts as an efficient light absorber [58] yet allowing the electrical carriers' drift.

Here, three new 2D HOIS based on the long-chain amine 2,2,4(*2,4,4*)-trimethyl-1,6-hexanediamine are presented. This amine is composed of a mixture of the 2,2,4- and 2,4,4-isomers, as acquired. It is interesting to study the formation of 2D HOIS where the organic spacer, such as this one, first alters its conformation slightly as a double-

protonated salt compared to its free-standing form, and second its conformation with the methyl groups around its carbon backbone presents a packing problem in order to support the naturally forming 2D inorganic structures. In fact, both isomers unfold slightly when protonated, however, their length is slightly different between the two isomers according to the ab initio calculations presented herein, due to the distance of the 2 methyl groups from the nitrogen atom. It is expected that the final 2D hybrid material could contain a mixture of the isomers as organic spacers. It is also possible that these could aggregate in 2,4,4- and 2,2,4-rich crystal domains. This is particularly favorable for the iodine compound where the large I–Pb–I lengths allow for more packing possibilities of the organic spacer which needs to grasp the inorganic layer at every apical iodine via electrostatic bonds. The synthesis, crystal structure and some optoelectronic properties of [2,2,4(*2,4,4*)-trimethyl-1,6-hexanediamine]PbX_4 (X = I, Br, Cl) are reported and discussed. It is important to note that both the 2,2,4 and 2,4,4 isomers most probably are composed of equal amounts of enantiomers, thus, it is expected that this underlying chirality also plays a crucial role for both structure and optical properties. To our knowledge, there is no report concerning the chirality of this particular amine. Also, related preliminary studies of their optical properties did not reveal strong chiral properties. Finally, the optical properties of the here reported materials display all the characteristic novel phenomena of the 2D hybrid lead halide semiconductors, however, the excitonic peaks observed are broadened and diminished in intensity.

Experimental section

Starting materials

The following materials were used as received without any further purification; lead(II) iodide 99% (Sigma-Aldrich 211168), lead(II) bromide 98%+ (Sigma-Aldrich 211141), lead(II) chloride (Alfa 21490), 2-2-4(*2,4,4*)-trimethyl-1,6-hexanediamine 99% (Sigma-Aldrich 722650), 57% aqueous hydroiodic acid (Sigma-Aldrich 210021), 48% aqueous hydrobromic acid (Alfa-Aesar 14036), 37% aqueous hydrochloric acid (Sigma-Aldrich 320331), anhydrous acetonitrile (Sigma-Aldrich 34851), dimethyl sulfoxide 99.9% (DMSO, Sigma Aldrich 276855) and *N,N*-dimethylformamide (DMF, Sigma-Aldrich 68-12-2).

Synthesis of 2,2,4*(2,4,4)*-trimethyl-1,6-hexanediamine lead halide materials

Synthesis of (2,2,4*(2,4,4)*-trimethyl-1,6-hexanediamine)PbI_4 (m1):

240 μL of 2,2,4(*2,4,4*)-trimethyl-1,6-hexanediamine (1.3 mmol) was mixed with 300 μL of 57% aqueous hydroiodic acid (2.2 mmol). 0.461 g of PbI_2 (1 mmol) was dissolved in a mixture of 1.2 mL CH_3CN and 60 μL of HI (0.45 mmol). The two solutions were mixed under stirring at 40 ^oC until dark orange-reddish crystals were formed by slow solvent evaporation. Other approaches to synthesize variants of this compound (denoted as **m1_ns/2/3/4**) were investigated and described in detail in the Supporting Information available online, which provide similar peaks in the low angle XRD patterns.

Synthesis of (2,2,4*(2,4,4)*-trimethyl-1,6-hexanediamine)$PbBr_4$ (m2):

362 μL of 2,2,4(*2,4,4*)-trimethyl-1,6-hexanediamine (2 mmol) and 120 μL of 48% aqueous hydrobromic acid was mixed (1 mmol). 0.734 g of $PbBr_2$ (2 mmol) was dissolved in a mixture of 800 μL CH_3CN and 0.5 mL of HBr (4.4 mmol). The two

solutions were stirred at 40 ^{o}C. From the final solution the solvent was slowly evaporated until a white powder formed.

Synthesis of (2,2,4*(2,4,4)*-trimethyl-1,6-hexanediamine)$PbCl_4$ (m3):

181 μL of 2,2,4(*2,4,4*)-trimethyl-1,6-hexanediamine (1 mmol) and 40 μL of 37% aqueous hydrochloric acid was mixed (0.47 mmol). 0.278 g of $PbCl_2$ (1 mmol) was dissolved in a mixture of 1.2 mL DMSO and 40 μL of HCl(0.47 mmol). The two solutions were mixed under stirring at 40 ^{o}C until a white precipitate was formed. The solution was left to dry by slow evaporation of the solvent.

X-ray powder diffraction

The X-ray powder diffraction data (XRPD) was obtained from polycrystalline samples at room temperature on a Bruker D8 Advance diffractometer equipped with a LynxEye® detector and Ni-filtered Cu$K\alpha$ radiation. The scanning area covered the 2θ range of 2–80°, with a scanning angle step size of 0.015° and a time step of 0.161 s. Structural analysis was carried out using the FULLPROF software [59].

Scanning Electron Microscopy and EDX

The SEM images and EDX data was recorded on an EVO-MA 10 Carl Zeiss instrument equipped with a 129 eV resolution INCAx-act Silicon Drift Detector. EDX spectra were acquired at 15 kV and images at 5 kV accelerating voltage.

Optical measurements

The UV/Vis optical absorption (OA) spectra were recorded on a UV-1800 UV Shimadzu spectrophotometer in the range of 200–800 nm, at a sampling step of 0.5 nm using 1.5 nm slits, a combination of halogen and D2 lamps as sources. The samples were measured as thin or thick spin-coated films on quartz or ITO substrates, after subtracting the substrate's spectra as reference. The photoluminescence (PL) and

photoluminescence excitation (PLE) spectra were obtained from thick deposits on quartz plates, mounted in a Hitachi F-2500 FL spectrophotometer employing a xenon 150 W lamp and an R928 photomultiplier. All the above data were obtained at room temperature. For the measurements at T = 77 K liquid N_2 was used as a blanket to a sealed quartz tube hosting the materials under argon atmosphere.

Results and Discussion

Crystal structures

The Powder XRD patterns of **m1**, **m2** and **m3** have been indexed, where all compounds crystallize with monoclinic symmetry with strong resemblance to the 2D hybrid semiconductor $[NH_3(CH_2)_6NH_3]PbI_4$ [60] which is presented in Fig. 1, and are presented in Fig. 2 along with the latter's compound computed XRD pattern. No peaks were assigned to unreacted $PbCl_2$, $PbBr_2$ or PbI_2. However, due to the low symmetry of the perovskite compounds and the lack of high-quality single crystals, the XRPD patterns are not suitable for a full structural Rietveld analysis to determine the atomic positions.

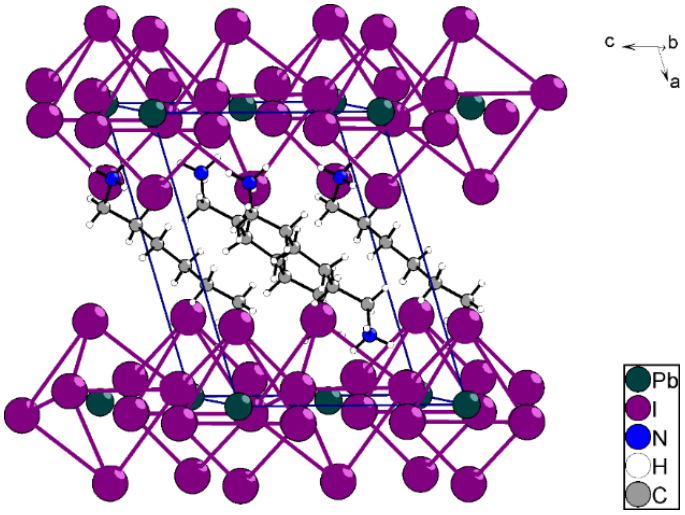

Figure 1. Crystal structure of $[NH_3(CH_2)_6NH_3]PbI_4$ from ref. [60] (COD ID 7203879). Unit cell edges are denoted with dark blue lines, whereas the corner-sharing $[PbI_6]^{4-}$ octahedra edges are denoted with violet lines.

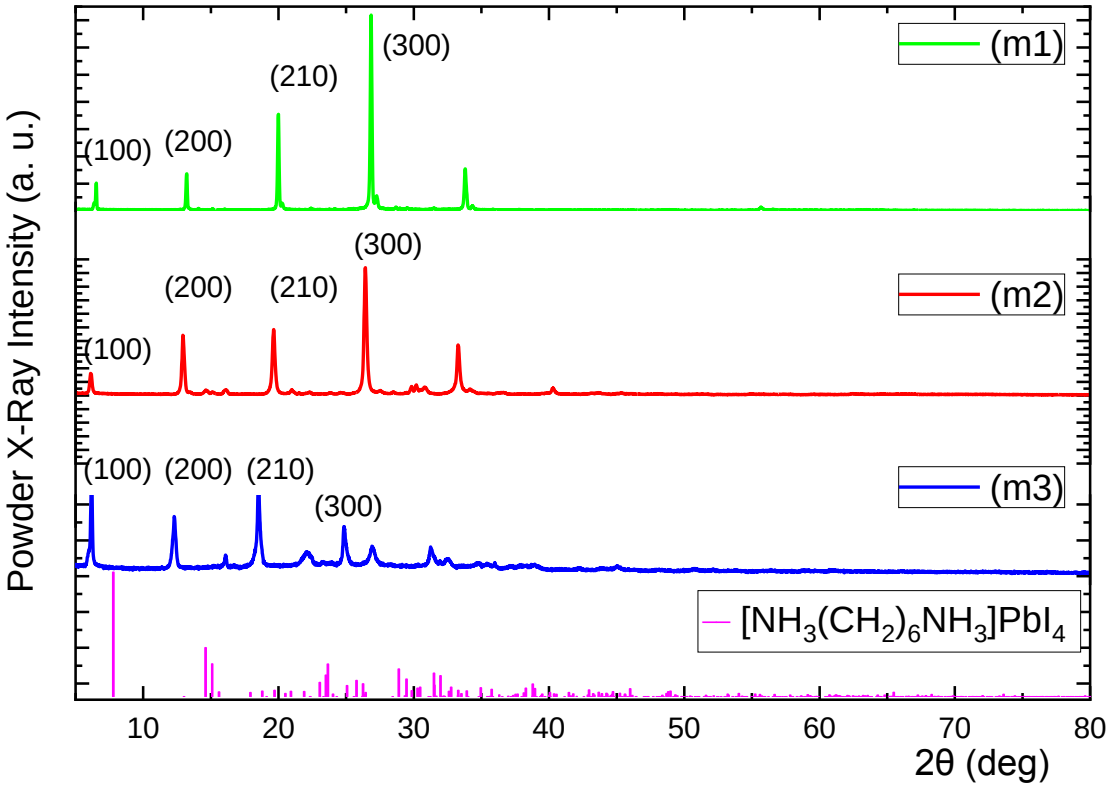

Figure 2. Powder XRD patterns with normalized diffraction intensities at room temperature for **m1** (green), **m2** (red) and **m3** (blue) and the computed powder XRD of the compound in Fig. 1 (magenta).

Peaks at 2θ of ca. 6^{o} and ca. $12^{o}\pm0.1°$ are associated with the inorganic interlayer distance of the 2D perovskites according to literature [61–63] and assigned to the (100) and (200) planes, respectively, in compounds **m1**, **m2** and **m3**. It is worth noting that the position of these peaks is almost independent from the choice of the halogen atom since the interlayer distance, giving rise to the strongest XRD peak, is mostly affected by the organic spacer and not by the halogen atom. As 2,2,4*(2,4,4)*-trimethyl-1,6-hexanediamine is significantly bulkier than the 1,6-hexanediamine,

larger d-spacings are expected for the (*h00*) reflections (assuming that *a* axis is vertical to the inorganic layers), thus, shifting the 2θ angles to lower values than in $[NH_3(CH_2)_6NH_3]PbI_4$. Very recently, a similar 2D crystal structure was reported for the 2D-$(MBA)_2PbI_4$ (MBA = chiral R/S-methylbenzylammonium) which produces a similar diffraction pattern to the title compounds [64] as well as a similar work by Ma et. al. [65] where chirality further induces more exotic light-matter interaction phenomena.

The amine configuration has been optimized with ab initio dynamics (Tables 2 and 3, See Supporting Information) in order to check for self-consistency in the XRD large plane spacings. The computed average protonated amine lengths plus the halogen-Pb-halogen distances amounts to almost the experimentally deduced *d* values, as derived from the first low angle peak in the Powder XRD patterns.

In Supporting Information, the Powder XRD patterns (Fig. S1, S5 and S9) for the iodine synthesis variations are presented. The low angle peaks presented, indicate in all cases a 2D superstructure. Sample **m1_ns3** (Fig. S5 see Supporting Information, which is similar to **m1** besides the extra HI and PbI_2 but within the ideal stoichiometry) has two sharp XRD peaks at low angles showing the formation of a unit cell with a smaller large axis by ca. 1.4 Å smaller. It is possible that this formation is due to the existence of two different phases derived from the 2,2,4 and 2,4,4 amine packings, which differ as found in the computed ab initio isomer lengths, described in the Supporting Information section as the distance between the N atoms on each isomer.

The as prepared powders of the materials were stored in the dark at room temperature for a period of three years. The samples were dried before characterizing them. Compound **m1** appeared to decompose at high drying temperatures (~70 ^oC). The **m2**

and **m3** materials were dehydrated by partial thermal treatment in a desiccator set at 120 ^{o}C, after which these were reversed possibly from hydrates to non-hydrates. The color of the powders did not change after the thermal treatment. Fig. 3 and Fig. 4 present the XRD patterns for compounds **m2** and **m3**, respectively, as prepared and after the aforementioned storage period and the thermal treatment. It is possible that H_2O molecules were partially intercalated in the perovskite structure, so that the organic-inorganic framework was retained, but the X-ray diffraction pattern became more diffuse, as in the case of $CH_3NH_3PbI_3$ upon hydration [66]. For both compounds the first low angle peak has become more intense and the other peaks seem to be minimized while new peaks have appeared. The normal degradation appears to induce change mostly to the inorganic layers, while the organic spacer is not altered significantly.

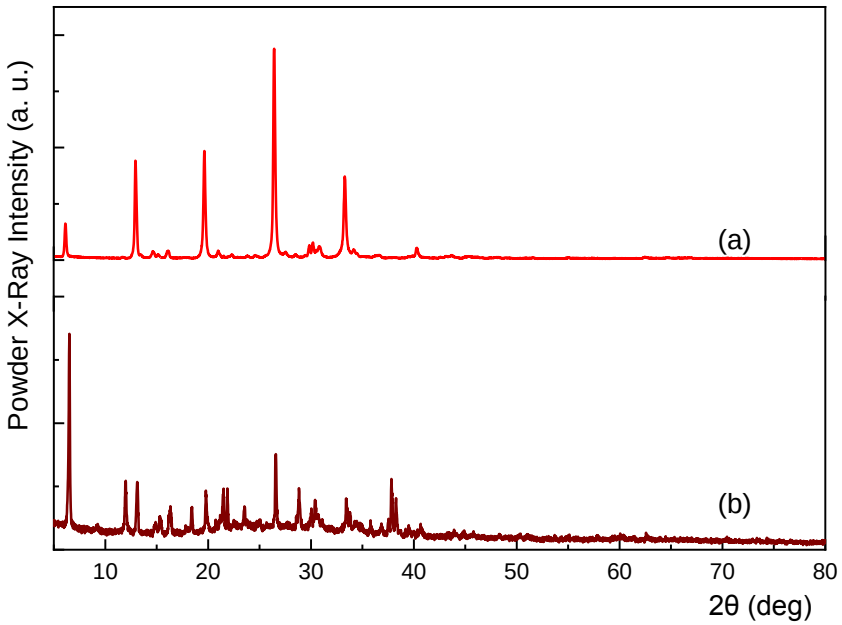

Figure 3. XRD patterns of **m2** (a) as prepared and (b) after three years.

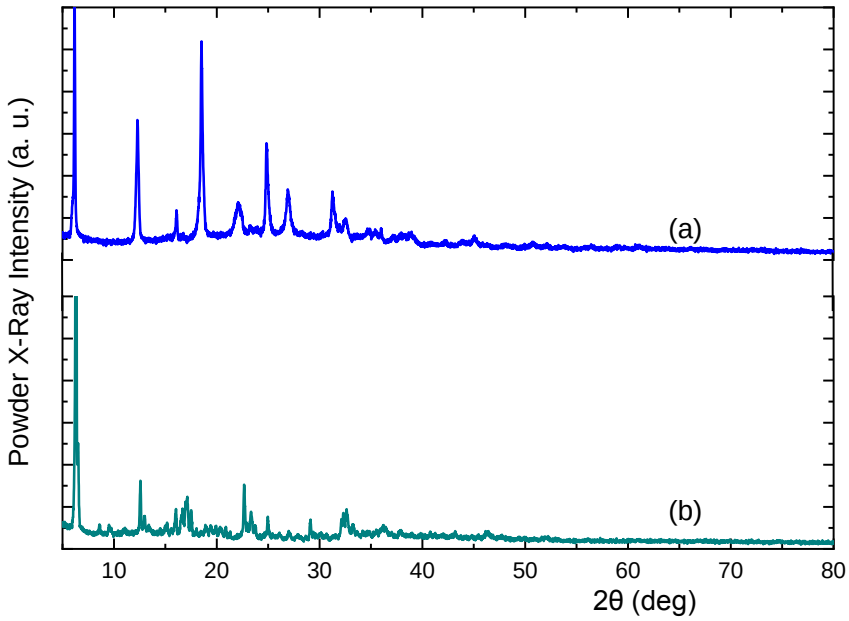

Figure 4. XRD patterns of **m3** (a) as prepared and (b) after three years.

Electron Microscopy

SEM images of all three compounds as prepared are presented in Supporting Information (Fig. S13). In particular, Fig. S13 (a–b), Fig. S13 (c–d) and Fig. S13 (e–f) show images of the as prepared compounds **m1**, **m2** and **m3**, respectively, where some pin holes are observed and a flower like structure, while it is also seen that the anion substitution alters the perovskite morphology. Compound **m1** forms a grain-like microstructure while its variants **m1_ns2** (Fig. S2) and **m1_ns3** (Fig. S6) form needles on top of the flower-like microstructure. The morphology of the variant **m1_ns4** appears to be plate-like (Fig. S10). On the contrary, compounds **m2** and **m3** form needle-like microstructures (Fig. S13). Should a synthesis proceed with a surplus of the amine and smaller quantity of hydroiodic acid, the material assumes a soft-plastic texture.

Comparison of the SEM images of **m2** and **m3** are presented further below, before and after the three-year storage period except for **m1** since it was the only one that

degraded beyond characterization capability. In Fig. 5, **m2** is presented, where after drying the samples a more well-formed cubic shaped microstructure is observed.

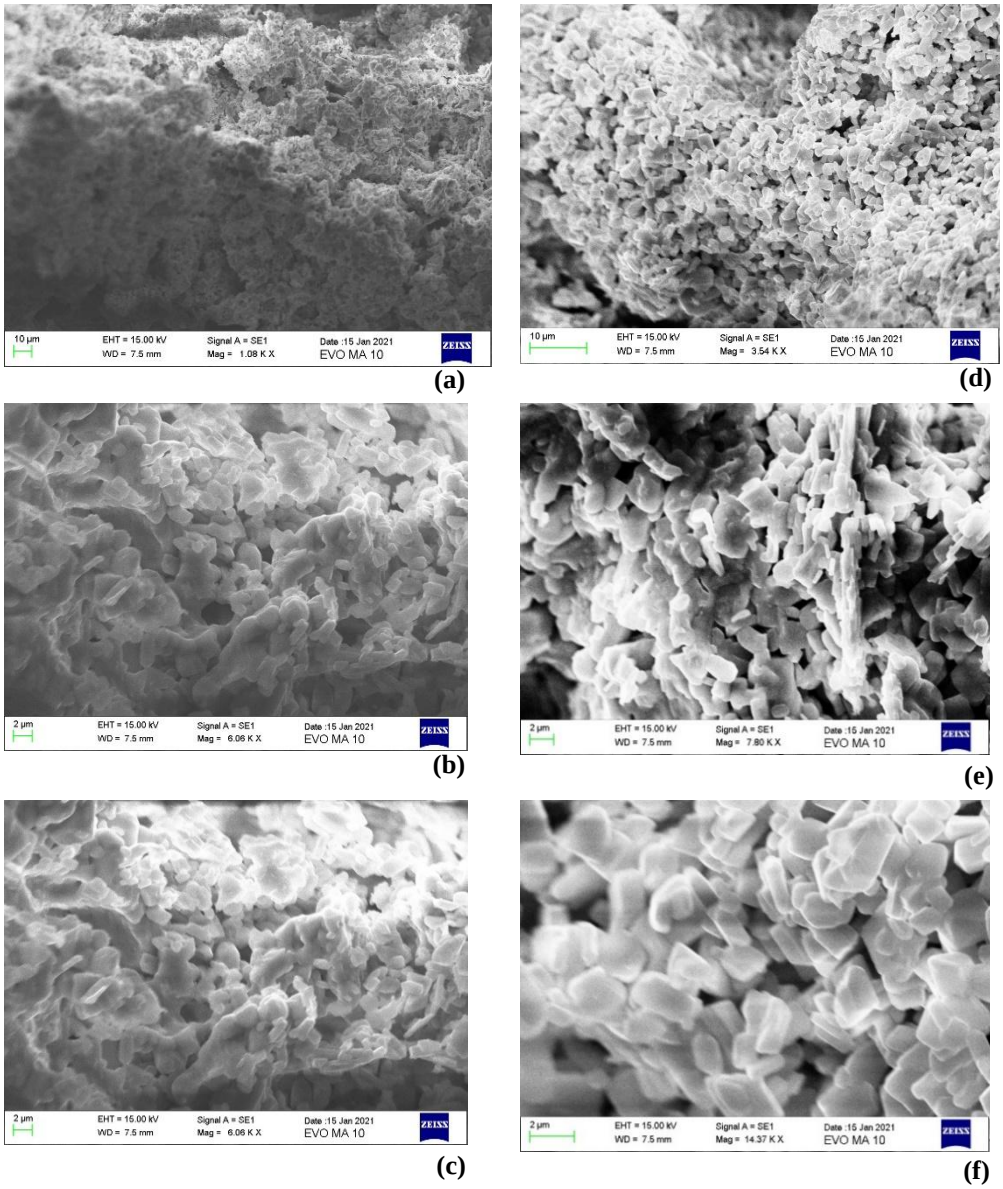

Figure 5. SEM images of **m2** as synthesized (a–c) and dried (d–f).

A comparison of the SEM images of **m3** (Fig. 6) allowed us to confirm that the morphology is quite similar except for some tetragonal particles observed in the as-synthesized compound (red circles). After drying and overnight storing of the

compound under vacuum, the small tetragonal units disappeared and a needle-like microstructure had formed.

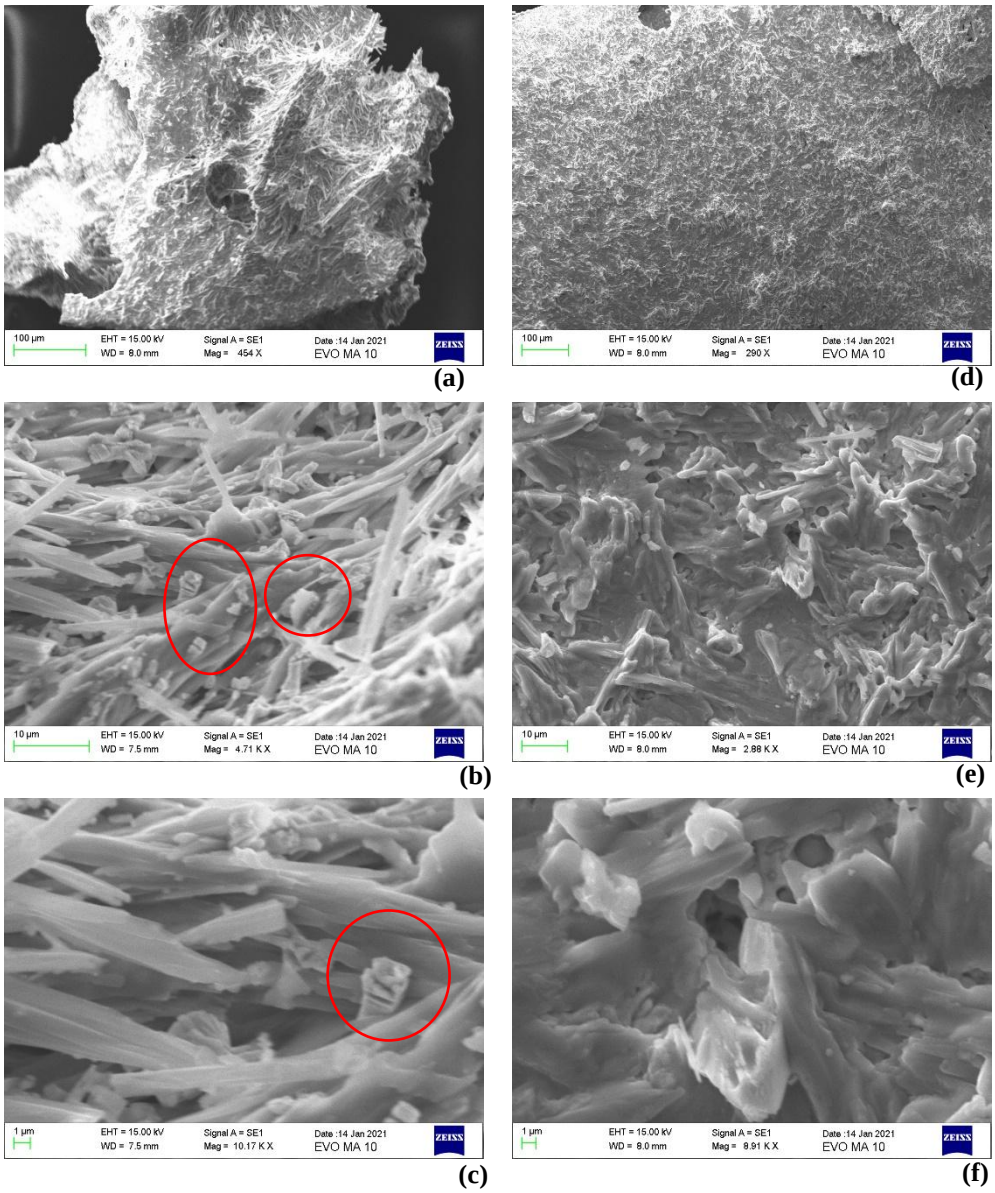

Figure 6. SEM images of **m3** as synthesized (a–c) and dried (d–f).

According to EDX measurements (Fig. S14–S16, Supporting Information), all compounds showed a molar ratio Pb:X (X = I, Br, Cl) of 1:4.This is in agreement with the results of the powder XRD measurements (Fig. 2) that indicate that the materials form 2D arrangements, where the corner-sharing topology leads to the aforementioned stoichiometry.

Optical Studies

The optoelectronic properties of the compounds were investigated using UV/Vis spectroscopy (Fig. 7) at room temperature. The optical absorption (OA) spectra reveal excitonic peaks at 494, 400 and 332 nm for compounds **m1**, **m2** and **m3**, respectively; for compound **m2** the peak is not as strong or sharp. Compound **m1** contains iodine which is larger and less electronegative than bromine and chlorine in compounds **m2** and **m3**, respectively, resulting to an excitonic red shift, in agreement with previous studies of similar compounds [**Error! Bookmark not defined.**, 67, 68]. In all three compounds, a second peak is observed at higher energies relative to the n = 1 excitonic peak. These low wavelength excitonic peak positions at 318 and 258 nm correspond to the absorption of the PbX_6^{4-} standalone units of the analogous Br and Cl compounds [69], respectively, which are, however, not completely isolated but slightly interact with the environment, as for example the isolated $PbBr_6^{4-}$ peak would be located at ca. 308 nm [70].

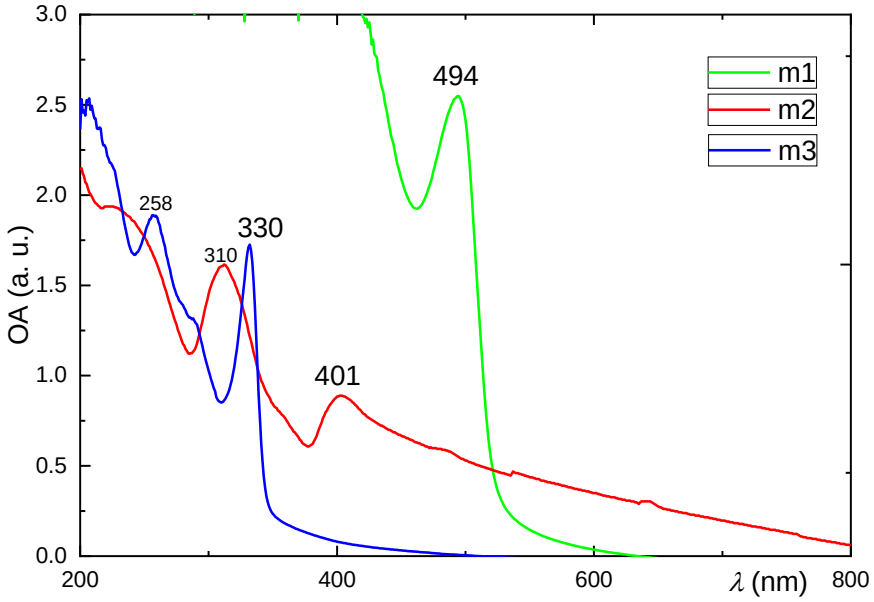

Figure 7. UV/Vis OA spectra of **m1**, **m2**, and **m3** as prepared.

The variant **m1_ns2** shows excitonic peaks at 487 nm (Fig. S3), due to the small amount of lead precursor used for this variant; possibly only small sized platelets formed leading to a considerable blue shift size effect. Sample **m1_ns4** exhibits peak at 502 nm (Fig. S11), that are slightly shifted relative to **m1**, which probably can be attributed to steric effects of the amine and "loose" hydrogen bonding and their modulation on energy band gaps of iodoplumbates [71, 72]. Variant **m1_ns3** exhibits excitonic peak at 363 nm (Fig. S7), as noted before, as well a weak 2D excitonic peak at 506 nm. This shows that minute changes, i.e.. doubling the HI moles, lead to the formation of 0D entities of the form PbI_6^{4-} and the minimization of the 2D inorganic sheets.

In Fig. 8, the UV/Vis spectra of **m2** as prepared aged samples are presented. The excitonic peak at ca. 400 nm is still present but the peak at 310 nm has strongly decreased, which implies that after the thermal dehydration of the stored compound **m2**, the peak corresponding to the 0D isolated lead bromide octahedra has been degraded, a phenomenon that has been observed before for similar compounds [73]. According to the SEM images (Fig. 5), **m2** after its long storage has in fact formed better crystals. Thus, the **m2** compound has not been degraded by oxygen and humidity, while compound **m3** has been affected as discussed further below.

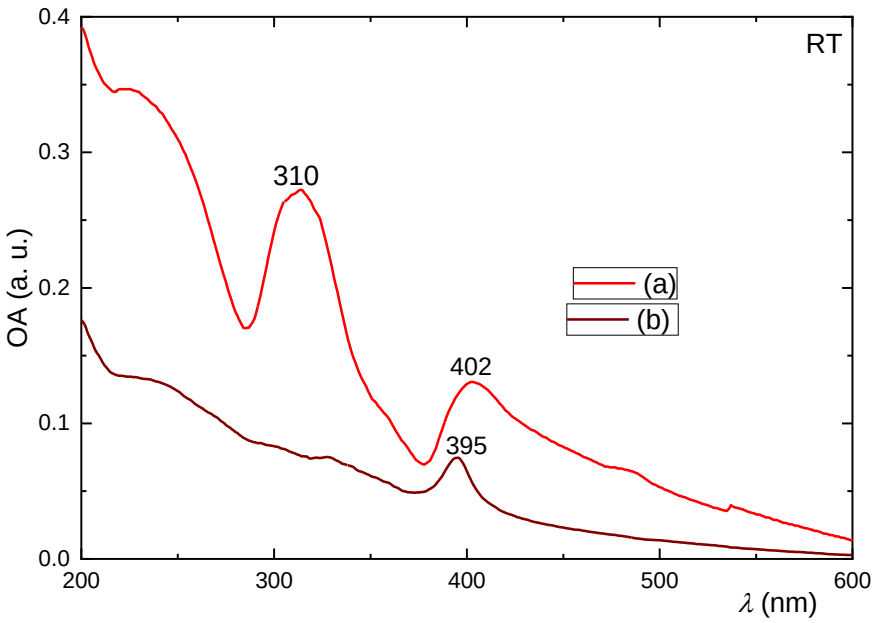

Figure 8. UV/VIS OA spectra of **m2** as prepared (a) and after three years storage (b).

A peculiar behavior is observed for compound **m3** after its prolonged storage. As it can be observed in Fig. 9, the peak at 332 nm has been minimized and the peak at 286 nm has been widened and enhanced, both remaining despite the loss of the 257 nm peak. It is possible that the 2D perovskite structure had its superstructure broken down along the long *a* axis to accommodate both the organic cation and any H_2O molecules trapped in between, and this has partially degraded the inorganic layers [74–76], since the organic spacer here is water soluble.

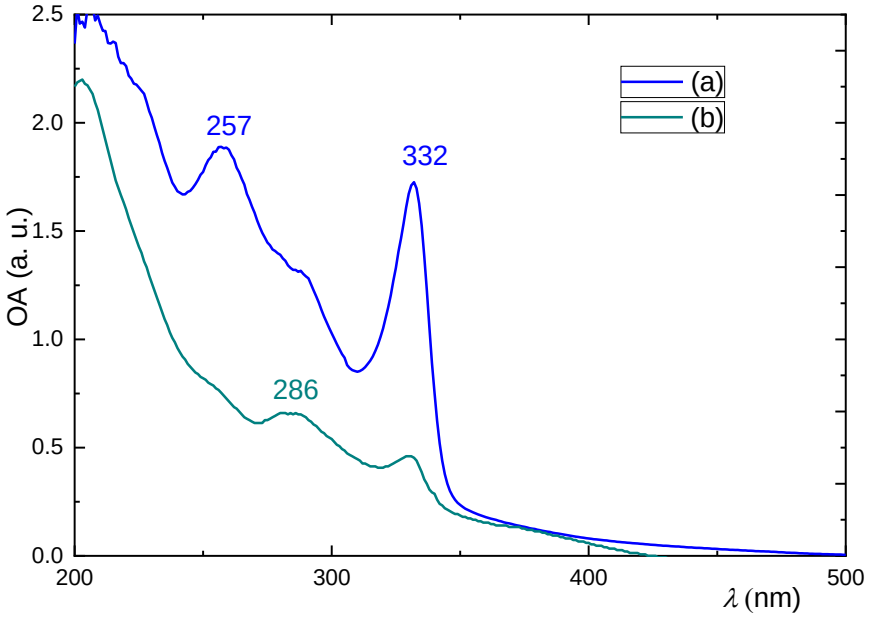

Figure 9. UV/VIS OA spectra of **m3** as prepared (a) and after three years storage (b).

By extrapolating the linear part of the Tauc graphs for the optical absorption, it is possible to get an estimate of the energy band gap values (Fig. S17; Supporting Information) of the as synthesized compounds **m1**, **m2** and **m3**; these were computed to be 2.82, 3.29 and 3.92 eV, respectively (see Supporting Information). Obtaining the energy band gap values in a different manner, from the first minimum of the OA spectra at higher energies than the excitonic peak, E_g values are estimated at 2.69, 3.28 and 4.0 eV for **m1**, **m2** and **m3**, respectively, leading to experimental excitonic binding energies of 185, 195 and 253 meV, respectively.

Fig. 10, Fig. 11 and Fig. 12 present the photoluminescence (PL) spectra of **m1**, **m2** and **m3**, respectively, while Fig. 13 and Fig. 14 compare the time variation of the PL of **m2** and **m3**, respectively, after their prolonged storage. In all three compounds, broad bands are observed rather than sharp excitonic peaks, before and after their storage. PL emission spectra exhibit excitonic broad bands as a double peak at 512

and 531 nm for **m1**, 414 nm for **m2** and 346 nm for **m3**. Comparing the OA and PL emission spectra, the excitonic peaks appear to have an average Stokes shift of 15 nm for all compounds, indicative of only few defect crystalline states of all compounds [77]. The double peak for **m1** is possibly due to two different variants, exhibiting, however, the same XRD pattern, or even more probably due to defects. It is interesting that the as prepared **m3** shows also a sharp peak at 400 nm and a broad one centered at 465 nm, both latter cannot be linked to other experimental observations of similar materials.

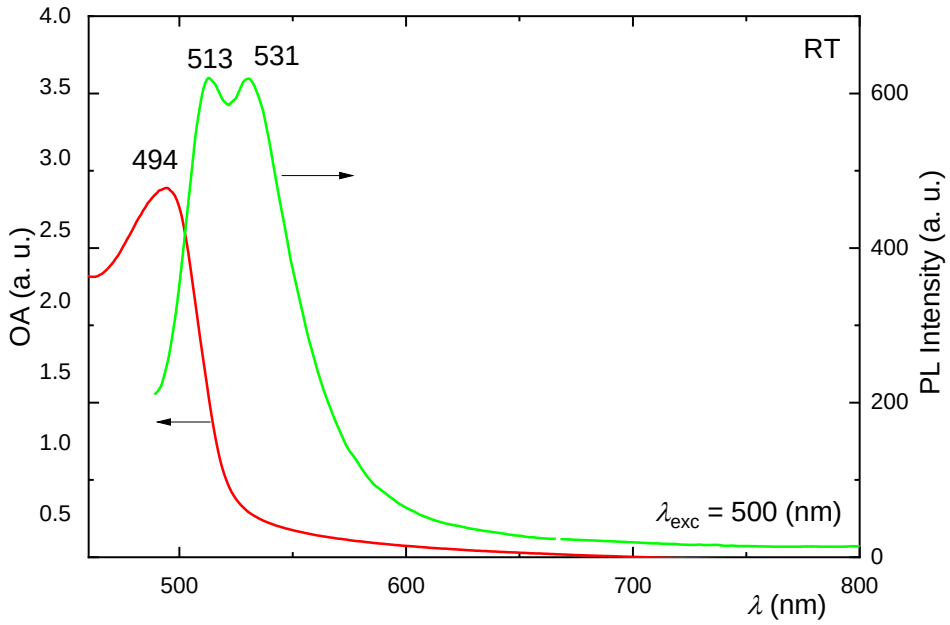

Figure 10. OA (red) and PL (green) spectra of **m1**.

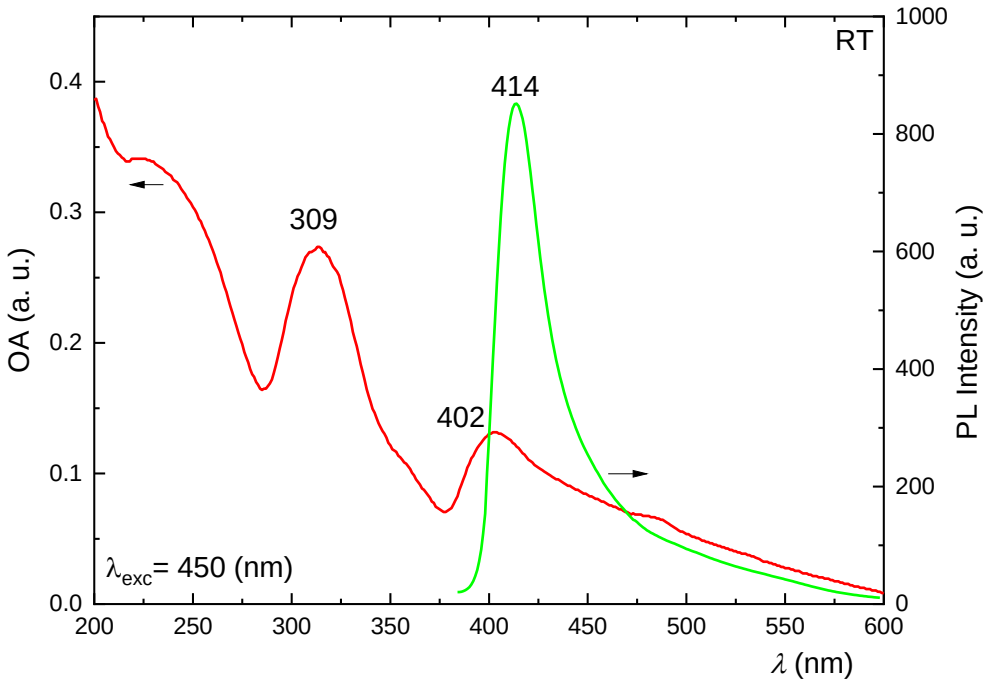

Figure 11. OA (red) and PL (green) spectra of **m2**.

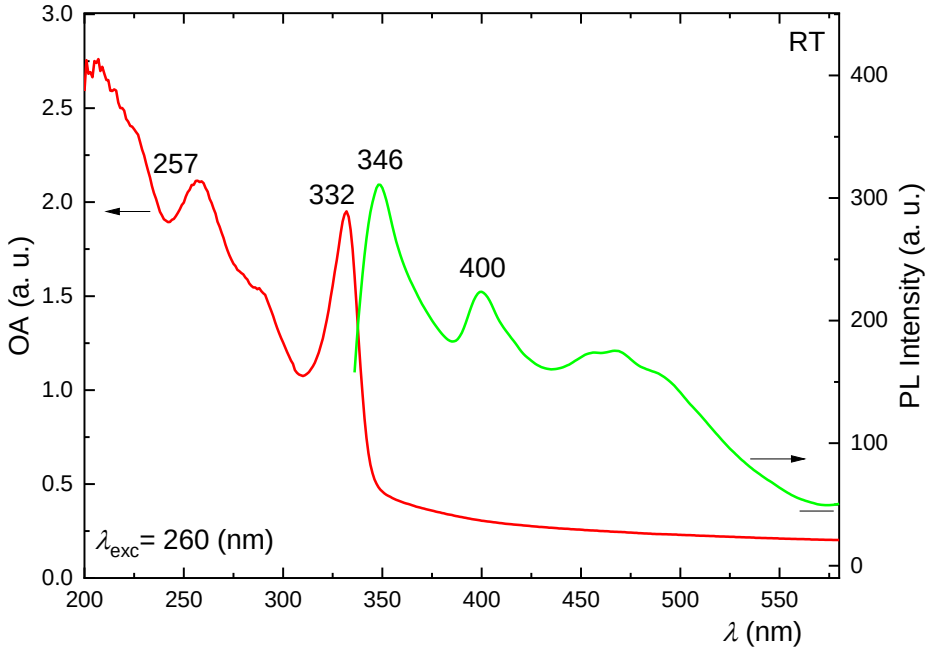

Figure 12. OA and PL spectra of **m3**.

As seen in Fig. 13, compound **m2**, presented minor alterations in the photoluminescence peaks after the three years storage period. A more intense and

sharper peak has appeared which is slightly blue-shifted to ca. 408 nm in contrast to the as prepared sample, ca. 414 nm, yet both spectra are quite wide. The PL spectra of the as prepared sample has been enhanced in order to be comparable to the aged one, which are comparable due to the similar geometry used for both.

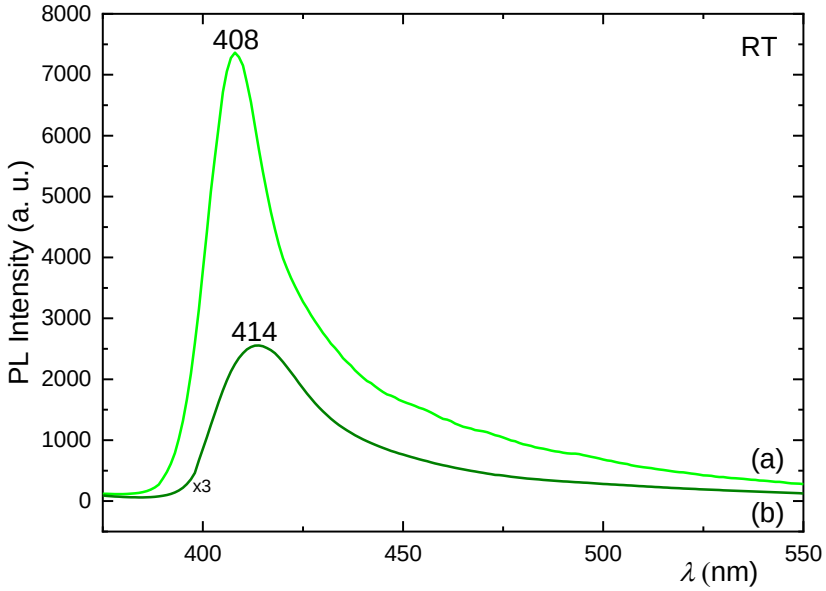

Figure 13. PL of **m2** as prepared (b) and after three years storage (a).

For compound **m3**, the PL spectra have revealed major differences after the three-year storage period (Fig. 14). According to the OA spectra, **m3** retains the 2D excitonic peaks, but the as prepared sample exhibits the PL peak at 347 nm, while the stored sample exhibits a broad and red-shifted excitonic PL peak to 363 nm, due to defects, and at the same time the 400 nm PL peak has disappeared. The PLE spectra, however, which should resemble the OA spectra, show that the spectra of both aged and fresh **m3** have a strong peak at 369 nm, probably denoting some defect states responsible for the low energy emission at 550 nm.

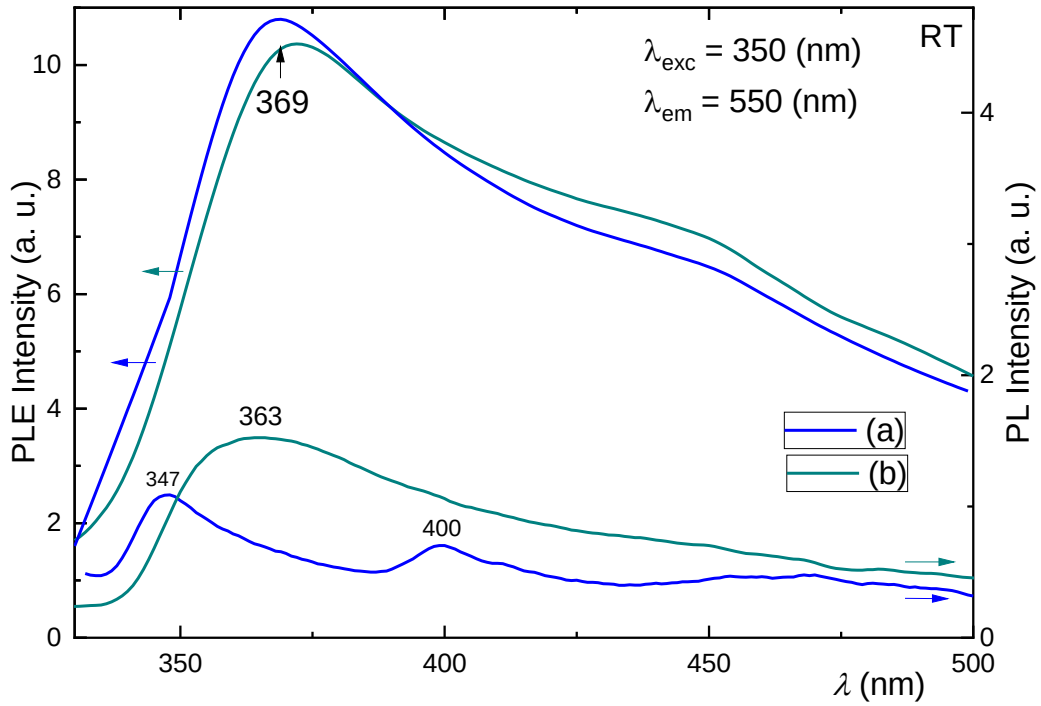

Figure 14. PLE (left) and PL (right) spectra of **m3** as prepared (a) and after three years (b).

In Fig. 15, 3D PL spectra of compound **m2** after being exposed to humidity and oxygen are presented. A blue up to green luminescence is observed that may be attributed to defects in the crystal structure in accordance to the data of Fig. 13. According to Fig. 6 the SEM images show more well-formed crystals with more sharp edges after the samples were exposed to humidity, as compared to the as synthesized sample which presents a smoother surface.

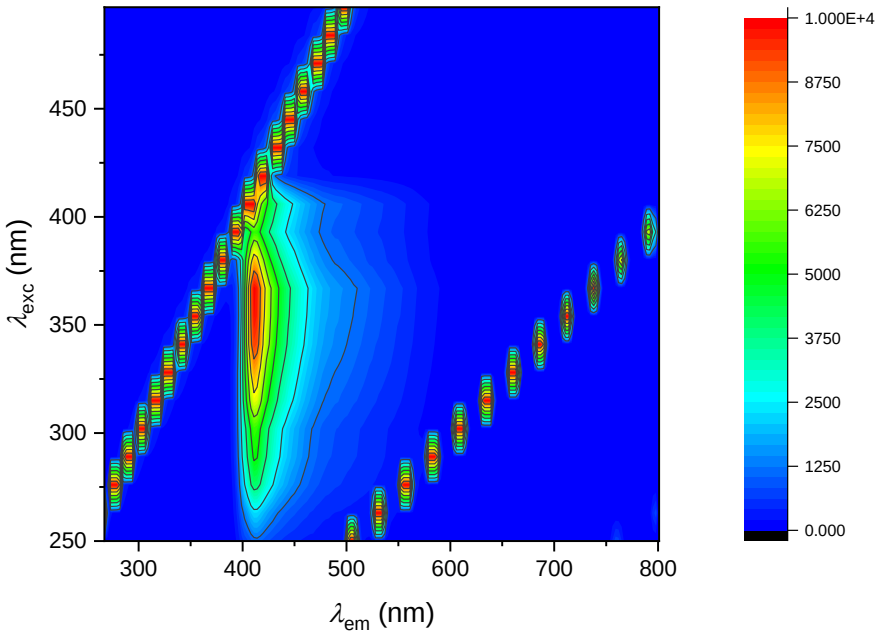

Figure 15. 3D PL spectra of **m2** at room temperature after 3 years.

In Fig. 16, 3D PL spectra of **m3** after being exposed to humidity and air are presented. A broad blueish-green luminescence is observed for a variety of excitation wavelengths from 260 nm up to 400 nm, evident of white like luminescence.

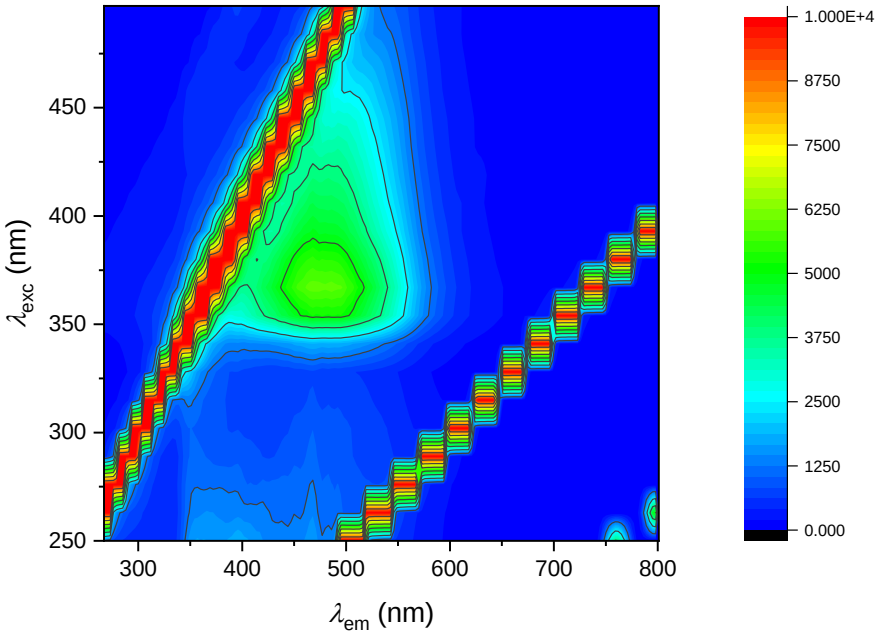

Figure 16. 3D PL spectra of **m3** at room temperature after 3 years storage.

In the Supporting Information, PL and PLE spectra of **m1_ns2**, **m2** and **m3** are provided, measured at 77 K for the as prepared compounds. These measurements were performed to investigate phenomena responsible for the low PL intensities observed compared to similar 2D lead halide perovskites. The PL spectra at 77 K of some of **m1_ns2** show a single peak at 509 nm (Fig. S18, Supporting Information), slightly blue-shifted in comparison to the RT spectra (Fig. S8, Supporting Information). These may be due to some structural variation, while the PLE spectra agree with the RT OA spectra as far as the exciton is concerned. The 77 K spectra of **m1_ns2** also display a shoulder at ca. 600 nm, probably due to complex defect states linked to the Pb^{+2} ion in a halogen environment, as for example seen in ref. [78]. Compound **m2** shows a peak at ca. 410 nm in the RT spectra (Fig. 11) as well as at 77K, however, the PLE spectra at 77K reveals a characteristic absorption at 300 nm (Fig. S19, Supporting Information) as well as a 368 nm PLE peak. The 300 nm PLE peak was used to collect a PL spectra with λ_{exc}=300 nm, that shows that at 77K this excitation yields a broad exciton peak centered at 407 nm as observed in Fig. S19 in Supporting Information. Exciting **m2** with higher or lower energies, i.e. 280 or 320 nm, provides PL spectra with less intensity than using 300 nm excitation. It is possible that the degraded **m2** has quantum confined sheets that instead of showing absorption at ca. 330 nm they have blue shifted at lower wavelengths, thus, using 300 nm radiation allows the broad 2D excitonic emission by virtue energy transfer. It is suggested that 300 nm radiation induces photoluminescence at high energies which is transferred to the remaining un-degraded 2D sheets to be emitted mainly as 407 nm radiation. In this process, all other radiative processes yield the broad PL peak of 407 nm. All these elucidate the complexity and role of the defects and multi-structural

diversity of the lead halide perovskites. It appears that this perovskite could emit broad UV-blue light if excited with a GaN LED or electrically activated.

Finally, **m3** shows an excitation dependent PL spectrum at 77K (Fig. S20, Supporting Information), centered far from the exciton peak at 500–560 nm, while the PLE spectrum reveals that absorptions at 303, 333, 368 nm appear to be responsible for this wide low temperature PL peak. It is conjectured that this PL behavior is due to a mechanism with which the exciton formed by the high energy excitation transfers its energy to defects of lower energy or transfer it towards the organic-inorganic artifacts which could form by lattice interruption introduced by the cooling process. Overall, it can be assessed that this type of materials, which deviate from the standard LD HOIS perovskites, have a quite complex behavior. Finally, it is important to note the similarity of the room temperature absorption spectra for the 2D materials in this work and those in refs. [64] and [65] based on RMX_4 which are broad rather than sharp as it usual observed in 2D lattices. It appears, however, that the usage of the mixture of 2,2,4 and 2,4,4 isomers as well as including their enantiomers provide a sharper exciton peak at 494 nm.

Conclusions

In the present paper, the synthesis of 2D lead halide perovskites using an isomer mixture of a diamine is presented. The as-synthesized materials were characterized in terms of their XRD patterns and their optical spectra. All materials appear to have less pronounced PL signals than the commonly known 2D perovskites, while in the case of the iodide, structural variants can be found. The compounds were stored in the dark under low humidity and re-examined after three years, where the iodine partially decomposed without retaining its properties. The bromide and chloride needed to be thermally treated to recover some of their properties. The chloride at room

temperature displays white-like luminescence which is desired for the use in OLEDs. It is suggested that the packing of the amines can in fact create variants in the iodine analogue, due to the larger number of packing possibilities while in the case of the bromine and chlorine the isomers build a 2D organic barrier which is the average of the two isomers. It is possible that this poor stacking as well as the bulky cation may create variations in the inorganic layer, partially responsible for the decreased PL intensities. Some discussion also includes the comparison of the results to other based on 2D chiral lead-iodide-based hybrid organic inorganic semiconductors.

Conflicts of interest

The authors declare that they have no conflicts of interest.

Acknowledgments: This research received partly funding from the European Union's Horizon 2020 program PeroCUBE through an Innovation Action under grant agreement no. 861985.

References

[1] Wells H. L. *Z. Anorg. Allg. Chem.* 1893, *3*, 195-210.
[2] Papavassiliou G.C. *Prog. Solid St. Chem. 1997, 25*, 125-270.
[3] Stranks S. D., Snaith H. J. *Nat. Nanotechnol*. 2015, *10*, 391-402.
[4] Chen J., Du W. N., Shi J. W., Li M. L., Wang Y., Zhang Q., Liu X. F. *InfoMat* 2019, *2*, 170-183.
[5] Wang R., Mujahid M., Duan Y., Wang Z., Xue J., Yang Y. *Adv. Funct. Mater.* 2019, *29*, 1808843 (25 pages).
[6] Zhang J., Yang X., Deng H., Qiao K., Farooq U., Ishaq M., Yi F., Liu H., Tang J., Song H. *Nano-Micro Lett.* 2017, *9*, 36 (26 pages).
[7] Hwang J., Rao R. R., Giordano L., Katayama Y., Yu Y., Shao-Horn Y. *Science* 2017, *358*, 751–756.
[8] Royer S., Duprez D., Can F., Courtois X., Batiot-Dupeyrat C., Laassiri S., Alamdari H. *Chem. Rev.* 2014, *20*, 10292–10368.
[9] Kojima, A., Teshima K., Shirai Y., Miyasaka T. *J. Am. Chem. Soc.* 2009, *17*, 6050–6051.
[10] https://www. nrel. gov/pv/assets/pdfs/best-research-cell-efficiencies. 20200406. pdf (accessed August 2021).
[11] Eperon G. E., Leijtens T., Bush K. A., Prasanna R., Green T., Wang J. T. -W., McMeekin D. P., Volonakis G., Milot R. L., May R., Palmstrom A., Slotcavage D. J.,

Belisle R. A., Patel J. B., Parrott E. S., Sutton R. J., Ma W., Moghadam F., Conings B., Babayigit A., Boyen H. -G., Bent S., Giustino F., Herz L. M., Johnston M. B., McGehee M. D., Snaith H. J. *Science* 2016, *6314*, 861–865.
[12] McMeekin D. P., Sadoughi G., Rehman W., Eperon G. E., Saliba M., Horantner M. T., Haghighirad A., Sakai N., Korte L., Rech B., Johnston M. B., Herz L. M., Snaith H. J. *Science* 2016, *351*, 151-155.
[13] Karani A., Yang L., Bai S., Futscher M. H., Snaith H. J., Ehrler B., Greenham N. C., Di D. *ACS Energy Lett.* 2018, *3*, 869-874.
[14] Mazzarella L., Lin Y., Kirner S., Morales-Vilches A. B., Korte L., Albrecht S., Crossland E., Stannowski B., Case C., Snaith H. J., Schlatmann R. *Adv. Energy. Mater.* 2019, *14*, 1803241.
[15] Young K., Yang T. Y., Suhonen R., Kemppainen A., Hwang K., Jeon N. J., Seo J. *Nat Commun* 2020, *11*, 5146-5156.
[16] Li H., Zuo C., Scully A. D., Angmo D., Yang J., Gao M. *Flexible Printed Electron.* 2020, *5*, 014006 (39 pages).
[17] Gusain A., Thankappan A., Thomas S. *J. Mater. Sci.* 2020, *55*, 13490–13542.
[18] Qiu L., Deng J., Lu X., Yang Z., Peng H. *Ang. Chemie Int. Edition* 2014, 53, 1-5
[19] Lee M., Ko Y., Jun Y., *J. Mater. Chem. A* 2015, 3, 19310-19313.
[20] Huang X., Huang X., Guo Q., Yang D., Xiao X., Liu X., Xia Z., Fan F., Qiu J., Dong G. *Nat. Photonics* 2020, *14*, 82–88.
[21] Hu J., Wang C., Qiu S., Zhao Y., Gu E., Zeng L., Yang Y., Li C., Liu X., Forberich K., Brabec C. J., Nazeeruddin M. K., Mai Y., Guo F. *Adv. Energy Mater.* 2020, *10*, 2000173 (53 pages).
[22] Li Z., Li Z., Li P., Chen G., Cheng Y., Pi X., Yu X., Yang D., Han L., Zhang Y., Song Y. *ACS Appl. Mater. Interfaces* 2020, *12*, 39082–39091.
[23] Nikolaou P., Vareli I., Deskoulidis E., Matsoukas J., Vassilakopoulou A., Koutselas I., Topoglidis E. *J. Solid. State Chem.* 2019, *273*, 17-24.
[24] Liu Y., Zheng Y., Zhu Y., Ma F., Zheng X., Yang K., Zheng X., Xu Z., Ju S., Zheng Y., Guo T., Qian L., Li F. *ACS Appl. Mater. Interfaces* 2020, *12*, 39649–39656.
[25] Tiley R. J. D. *Perovskites Structure-Property Relationships*, John Wiley & Sons: Hoboken 2016
[26] Eperon G. E., Stranks S. D., Menelaou C., Johnston M. B., Herz L. M., Snaith H. J. *Energy Environ. Sci.* 2014, *7*, 982-988.
[27] Li Y., Liu F. Z., Waqas M., Leung T. L., Tam H. W., Lan X. Q., Tu B., Chen W., Djurisic A. B., He Z. B. *Small Methods* 2018, 1700387 (27 pages).
[28] Hong K., Le Q. V., Kim S. Y., Jang H. W. *J. Mater. Chem. C* 2018, *6*, 2189-2209.
[29] Mohd Yusoff A. R. B., Gao P., Nazeeruddin M. K. *Coord. Chem. Rev.* 2018, *373*, 258-294.
[30] Ogomi Y., Morita A., Tsukamoto S., Saitho T., Fujikawa N., Shen Q., Toyoda T., Yoshino K., Pandey S. S., Ma T., Hayase S. *J. Phys. Chem. Lett.* 2014, *5*, 1004-1011.
[31] Stoumpos C. C., Malliakas C. D., Kanatzidis M. G. *Inorg. Chem.* 2013, *52*, 9019-9038.
[32] Shamsi J., Urban A. S., Imran M., Trizio L. D., Manna L. *Chem. Rev.* 2019, *119*, 3296-3348.
[33] Dai X., Xu K., Wei F. *Beilstein J. Nanotechnol.* 2020, *11*, 51-60.
[34] Li X., Zhang F., He H., Berry J. J., Zhu K., Xu T. *Nature* 2020, *578*, 555-558.
[35] Gao P., Grätzel M., M. K. Nazeeruddin *Energy Environ. Sci.* 2014, *7*, 2448-2463.
[36] Yin W., Yang J., Kang J., Yan Y., Wei S. *J. Mater. Chem. A* 2015, *3*, 8926-8942.

[37] Chen Q., Marco N. D., Yang Y. M., Song T. B., Chen C. C., Zhao H., Hong Z., Zhou H., Yang Y. *Nano Today* 2015, *10*, 355-396.
[38] Mercier N. *Angew. Chem. Int. Ed. 2019, 58*, 2–8.
[39] Saparov B., Mitzi D. B. *Chem. Rev.* 2016, *116*, 4558-4596.
[40] Lin H., Zhou C., Tian Y., Siegrist T., Ma B. *ACS Energy Lett.* 2018, *3*, 54-62.
[41] Kahwagi R. T., Thornton S. T., Smith B., Koleilat G. I. *Front. Optoelectron.* 2020, *13*, 196-224.
[42] Papavassiliou G. C., Koutselas I. B. *Synth. Met.* 1995, *71*, 1713-1714.
[43] Hong K., Van Le Q., Kim S. Y., Jang H. W. *J. Mater. Chem. C*. 2018, *6*, 2189-2209.
[44] Abbas M. S., Hussain S., Zhang J., Wang B., Yang C., Wang Z., Wei Z., Ahmad R. *Sustainable Energy Fuels* 2020, *4*, 324-330.
[45] Seok S. I., Kim B. *Energy Environ. Sci.* 2020, *13*, 805-820.
[46] Hautzinger M. P., Pan D., Pigg A. K., Fu Y., Morrow D. J., Leng M., Kuo M. Y., Spitha N., Lafayette D. P., Kohler D. D., Wright J. C., Jin S. *ACS Energy Lett.* 2020, *5*, 1430-1437.
[47] Li X., Fu Y., Pedesseau L., Guo P., Cuthriell S., Hadar I., Even J., Katan C., Stoumpos C. C., Schaller R. D., Harel E., Kanatzidis M. G. *J. Am. Chem. Soc.* 2020, *142*, 11486-11496.
[48] Masada S., Yamada T., Tahara H., Hirori H., Saruyama M., Kawasaki T., Sato R., Teranishi T., Kanemitsu Y. *Nano Lett.* 2020, *5*, 4022-4028.
[49] Chu Z., Zhao Y., Ma F., Zhang C. X., Deng H., Gao F., Ye Q., Meng J., Yin Z., Zhang X., You J. *Nat. Commun.* 2020, *11*, 4165 (8 pages).
[50] Fu Y., Jiang X., Li X., Traore B., Spanopoulos I., Katan C., Even J., Kanatzidis M. G., Harel E. *J. Am. Chem. Soc.* 2020, *142*, 4008-4021.
[51] Smith M. D., Connor B. A., Karunadasa H. I. *Chem. Rev.* 2019, *119*, 3104−3139.
[52] Mao L., Stoumpos C. C., Kanatzidis M. G. *J. Am. Chem. Soc.* 2019, *141*, 1171−1190.
[53] Leblanc A., Mercier N., Allain M., Dittmer J., ., Fernandez V., Boucher F., Kepenekian M., Katan C. *ACS Appl. Mater. Interfaces*, 2019, *11, 20743–20751.*
[54] Miyata K., Atallah T. L., Zhu X. Y. *Sci. Adv.* 2017, *3*, e1701469 (10 pages).
[55] Zhu H., Miyata K., Fu Y., Wang J., Joshi P. P., Niesner D., Williams K. W., Jin S., Zhu X. Y. *Science* 2016, *353*, 1409-1413.
[56] Hutter E. M., -Rueda M. C., Osherov A., ., Grozema F. C., Stranks S. D., Savenije T. J. *Nat. Mater.* 2017, *16*, 115-120.
[57] Zhu H., Trinh M. T., Wang J., Fu Y., Joshi P. P., Miyata K., Jin S., Zhu X. Y. *Adv. Mater.* 2017, *29*, 1603072 (6 pages).
[58] Lv Y., Ma H., Yin Y., Dong Q., Zhao W., Jinc S., Shi Y. *J. Mater. Chem. A* 2020,8, 10283-10290.
[59] Roisnel T., Rodriguez-Carvajal J. Fullprof, Version Sept. 2012, France
[60] Mousdis G. A., Papavassiliou G. C., Raptopoulou C. P., Terzis A. *J. Mater. Chem.* 2000, *10*, 515-518.
[61] Jia G., Shi Z. J., Xia Y. D., Wei Q., Chen Y. H., Xing G. C., Huang W. *Opt. Express* 2018, *26*, A66-A74.
[62] Cortecchia D., Neutzner S., Kandada A. R. S., Mosconi E., Meggiolaro D., De Angelis F., Soci C., Petrozza A. *J. Am. Chem. Soc*. 2017, *139*, 39-42.
[63] Lin C. W., Liu F., Chen T. Y., Lee K. H., Chang C. K., He Y., Leung T. L., Ng A. M. C., Hsu C. H., Popović J., Djurišić A., Ahn H. *ACS Appl. Mater. Interfaces* 2020, *12*, 5008-5016.

[64] Lu Y., Wang Q., Chen R., Qiao L., Zhou F., Yang X., Wang D., Cao H., He W., Pan F., Yang Z., Song C. *Adv. Funct. Mater*. 2021, 2104605 (7 pages).
[65] Ma J., Fang C., Chen C., Jin L., Wang J., Wang S., Tang J., Li D. *ACS Nano* 2019, *13*, 3659-3665.
[66] Arakcheeva A., Chernyshov D., Spina M., Forro L., Horvath E. *Acta Crystallogr., Sect. B: Struct. Sci., Cryst. Eng. Mater.* 2016, *72*, 716–722.
[67] Papavassiliou G. C., Mousdis G. A., Koutselas I. B. *Adv. Mater. Opt. Electron*. 1999, *9*, 265-271.
[68] Mousdis G. A., Papavassiliou G. C., Terzis A., Raptopoulou C. P. *Z. Naturforsch.* 1998, *53b*, 927-931.
[69] Papavassiliou G. C. *Prog. Solid State Chem.* 1997, *25(3-4)*, 125–270.
[70] Zhang L., Ju M. G., Liang W. *Phys. Chem. Chem. Phys*, 2016, *18*, 23174-23183.
[71] Nagasaka H., Yoshizawa-Fujita M., Takeoka Y., Rikukawa M. *ACS Omega* 2018, *3*, 18925-18929.
[72] Yu T., Zhang L., Shen J., Fu Y., Fu Y. *Dalton Trans.* 2014, *43*, 13115-13121.
[73] Van Gompel W. T. M., Herckens R., Van Hecke K., Ruttens B., D'Haen J., Lutsen L., Vanderzande D. *ChemNanoMat* 2019, *5*, 323 – 327.
[74] Mosconi E., Azpiroz J. M., De Angelis F. *Chem. Mater.* 2015, *27*, 4885-4892
[75] Christians J. A., Herrera P. A. M., Kamat P. V. *J. Am. Chem. Soc.* 2015, *137*, 1530-1538.
[76] Bonadio A., de Oliveira L. S., Polo A. S., Souza J. A. *CrystEngComm.* 2019, *21*, 7365-7372.
[77] Smith M. D., Watson B. L., Dauskardt R. H., Karunadasa H. I. *Chem. Mater.* 2017, *29*, 7083-7087.
[78] Novosad. S. S *Optics and Spectroscopy* 2000, *88*, 522–526.